








A computational model-based analysis of basal ganglia pathway changes in Parkinson's disease inferred from resting-state fMRI

Oliver Maith¹  | Francesc Villagrasa Escudero¹  | Helge Ülo Dinkelbach¹  |
Javier Baladron¹ | Andreas Horn²  | Friederike Irmen²  | Andrea A. Kühn²  |
Fred H. Hamker¹ 

¹Department of Computer Science,
Chemnitz University of Technology,
Chemnitz, Germany

²Movement Disorders and Neuromodulation
Unit, Department for Neurology, Charité–
University Medicine Berlin, Berlin,
Germany

Correspondence

Fred H. Hamker, Department of Computer
Science, Chemnitz University of
Technology, Chemnitz, Germany.
Email: fred.hamker@informatik.tu-
chemnitz.de

Funding information

Deutsche Forschungsgemeinschaft, Grant/
Award Number: HA2630/11-1 (SPP 2041)

Abstract

Previous computational model-based approaches for understanding the dynamic changes related to Parkinson's disease made particular assumptions about Parkinson's disease-related activity changes or specified dopamine-dependent activation or learning rules. Inspired by recent model-based analysis of resting-state fMRI, we have taken a data-driven approach. We fit the free parameters of a spiking neuro-computational model to match correlations of blood oxygen level-dependent signals between different basal ganglia nuclei and obtain subject-specific neuro-computational models of two subject groups: Parkinson patients and matched controls. When comparing mean firing rates at rest and connectivity strengths between the control and Parkinsonian model groups, several significant differences were found that are consistent with previous experimental observations. We discuss the implications of our approach and compare its results also with the popular “rate model” of the basal ganglia. Our study suggests that a model-based analysis of imaging data from healthy and Parkinsonian subjects is a promising approach for the future to better understand Parkinson-related changes in the basal ganglia and corresponding treatments.

KEYWORDS

BOLD correlations, data fitting, firing rate, spiking neuron model

Abbreviations: AMPA, α -amino-3-hydroxy-5-methyl-4-isoxazolepropionic acid; BADS, Bayesian adaptive direct search; BOLD, blood oxygen level-dependent; CortexI, cortex population with inhibitory neurons; CV, coefficient of variation; DA, dopamine; DBS, deep brain stimulation; dSN, direct spiny projection neurons; dwMRI, diffusion-weighted magnetic resonance imaging; FDR, False discovery rate; fMRI, functional magnetic resonance imaging; GABA, gamma-aminobutyric acid; GPe, external globus pallidus; GPI, internal globus pallidus; iSN, indirect spiny projection neurons; MEFC, mean experimental functional connectivity; PD, Parkinson's disease; PPMI, disease progression marker initiative; rs-fMRI, resting-state functional magnetic resonance imaging; SC, structural connectivity; SNc, substantia nigra pars compacta; STN, subthalamic nucleus.

Edited by Yoland Smith.

The peer review history for this article is available at <https://publons.com/publon/10.1111/ejn.14868>

This is an open access article under the terms of the Creative Commons Attribution License, which permits use, distribution and reproduction in any medium, provided the original work is properly cited.

© 2020 The Authors. European Journal of Neuroscience published by Federation of European Neuroscience Societies and John Wiley & Sons Ltd

1 | INTRODUCTION

Neuroimaging methods have contributed greatly to the understanding of the human brain. Functional magnetic resonance imaging (fMRI) measures neuronal activation indirectly through changes in blood flow and oxygen saturation. In resting-state fMRI (rs-fMRI; Biswal, Zerrin Yetkin, Haughton, & Hyde, 1995; He et al., 2009), the spontaneous fluctuations of the blood oxygen level-dependent (BOLD) signal are measured while the subjects remain in a constant resting state. Then correlations of BOLD signals between different brain regions can be determined, which are called functional connectivity in the field of rs-fMRI (Friston, 2011). Although there is no direct link between these correlations of BOLD signals and the underlying neuronal connectivity or functionality, several studies showed that the spontaneous fluctuations of the BOLD signals have a neurophysiological basis (Biswal et al., 1995; Brookes et al., 2011; He, Snyder, Zempel, Smyth, & Raichle, 2008). Computational models have greatly complemented the analysis of functional connectivity (for a review see Popovych, Manos, Hoffstaedter, & Eickhoff 2019). Detailed biologically inspired models of the brain can be adjusted to reproduce the observable neuroimaging data and then can be examined in detail on various scales. Thus, this model-based analysis allows to extract information, such as connectivity strengths and spiking activity, that cannot be achieved from the imaging data alone. Several computational studies have demonstrated the potential of this approach (Cabral et al., 2013; Deco & Jirsa, 2012; Deco et al., 2013; Schirner, McIntosh, Jirsa, Deco, & Ritter, 2018; Schmidt et al., 2018; Van Hartevelt et al., 2014).

We here use these techniques to reveal more insight into functional connectivity changes induced by Parkinson's disease (PD), which is a neurological disorder characterized by numerous motor, but also non-motor symptoms (Jankovic, 2008). It is directly or indirectly resulting from the loss of dopaminergic cells in the substantia nigra pars compacta (SNc), which leads to a reduced level of dopamine (DA) in its target structures such as in the striatum and pallidum, main nuclei of the basal ganglia (Bernheimer, Birkmayer, Hornykiewicz, Jellinger, & Seitelberger, 1973), which in turn likely affects processing in the cortex–basal ganglia loops (for reviews Galvan, Devergnas, & Wichmann 2015; Nambu, Tachibana, & Chiken, 2015)). The findings about the changes in the basal ganglia due to PD have been integrated into conceptual models, such as the influential rate model of the basal ganglia (Albin, Young, & Penney, 1989; DeLong, 1990). As post hoc, conceptual models have less predictive power, neuro-computational models at different levels of detail have been developed to reveal further insight into differences between healthy and Parkinsonian states of processing within the basal ganglia (for reviews see Humphries,

Obeso, & Dreyer, 2018; Maia & Frank, 2011; Rubin, 2017; Schroll & Hamker, 2016).

In those models, a PD state has been either introduced by rules that affect the neural activity of striatal projection neurons dependent on DA or DA-dependent learning rules or by directly assuming changes in functional connectivity strengths. While those assumptions are generally well motivated by findings, the particular validity of each assumption is difficult to prove. Thus, the predictions made by these neuro-computational models with respect to how PD changes processing in the basal ganglia critically depend on assumptions built into the model about the Parkinsonian state.

Here, we present a completely different approach to explore PD-related changes in basal ganglia processing which is more data-driven. We fit a spiking neuro-computational model of the basal ganglia to experimental functional connectivity data from PD patients and control subjects. The data from PD patients have been previously obtained by Horn et al. (2019). Instead of including specific assumptions on DA deficiency in the basal ganglia in our model, we only assume that PD leads to altered connectivity in the basal ganglia. The connectivity parameters of the different connections of our spiking neuro-computational model are adjusted individually to match each PD patient's and control subject's functional connectivity data comprising the sensory-motor parts of the cortex, subthalamic nucleus (STN), striatum, internal and external globus pallidus (GPi, GPe) and thalamus providing us an individual model for each PD patient and control subject. While parameter fitting took place at the level of correlations in BOLD signals, we bridge scales and obtain individual spiking resting-state models of the cortex–basal ganglia motor loop. We analyze the data-induced computational differences between the control and patient group and compare them with the rate model of the basal ganglia (DeLong, 1990) and recent data.

2 | MATERIALS AND METHODS

2.1 | Data acquisition

The rs-fMRI data used here are from the PD patients in deep brain stimulation OFF condition (DBS OFF) and control subjects studied in resting state by Horn et al. (2019). Particularly, we look at (for each subject) the functional connectivity of the basal ganglia, thus the correlations between the BOLD time series obtained in the following brain areas of the motor brain: cortex, STN, striatum, GPe, GPi and thalamus. As these motor brain areas are symmetrical in the left and right hemisphere, our data consist of two functional connectivity matrices per subject, one related to these six brain areas on the left side and the other to the same brain areas on the right side of the brain.

TABLE 1 Parameter values for the neuron models

Population	a	b	c (mV)	d	C	I	n_0	n_1	n_2	SD_{SN}
Striatum	0.05	-20	-55	377	50	0.0	61.65	2.59	0.02	2
GPI	0.005	0.585	-65	4	1	30.0	140	5	0.04	3
GPe	0.005	0.585	-65	4	1	12.0	140	5	0.04	5
STN	0.005	0.265	-65	2	1	3.0	140	5	0.04	2
Thalamus	0.02	0.25	-65	0.05	1	3.5	140	5	0.04	2
Cortex	0.02	0.2	-72	6	1	50.0	140	5	0.04	10
CortexI	0.02	0.2	-72	6	1	0.0	140	5	0.04	0

In the study carried out by Horn et al. (2019), PD patients (20 in total, four of them were women) were scanned (with a repetition time of 2,690 ms) first during DBS ON and after an interval of 5–15 min with the impulse generator switched off (DBS OFF). Patients were 63 ± 6.6 ($M \pm SD$) years old when DBS surgery took place and they were scanned 30 ± 21 months after surgery with their usual medication ON (Levodopa). The rs-fMRI time series were detrended; noise related to motion, cerebrospinal fluid, and white-matter were removed; and a bandpass filter between 0.009 and 0.08 Hz was applied. For details about medication, patients' inclusion criteria, scanner, preprocessing of BOLD time series, voxel-wise parcellation and links to open sources please see Horn et al. (2019).

Controls (15 in total, four were female) were 59.5 ± 11.9 years old, and their rs-fMRI data were collected within Parkinson's Disease Progression Marker Initiative (PPMI) database (ppmi-info.org; Marek et al., 2011). These data were processed identically to the patients' data of the same study.

2.2 | Network description

We used a spiking neuro-computational model of the basal ganglia based on our previous work (Baladron, Nambu, & Hamker, 2019), but determined the connectivity parameters by an optimization procedure. The model is composed of several populations of spiking neurons, each representing a different nucleus of the basal ganglia, thalamus or cortex. The membrane potential of each cell is computed using the Izhikevich (2004) neuron model:

$$\begin{aligned}
 \frac{dV}{dt} &= n_2 V^2 + n_1 V + n_0 - U/C - g_{\text{AMPA}} (V - E_{\text{AMPA}}) - g_{\text{GABA}} (V - E_{\text{GABA}}) + I + \mu \\
 \frac{dU}{dt} &= a(bV - U) \\
 \tau_{\text{AMPA}} \frac{dg_{\text{AMPA}}}{dt} &= -g_{\text{AMPA}} \\
 \tau_{\text{GABA}} \frac{dg_{\text{GABA}}}{dt} &= -g_{\text{GABA}} \\
 \tau_{\mu} \frac{d\mu}{dt} &= -\mu + SN \\
 \text{if } V \geq 30 \text{ mV, then } &\begin{cases} V \leftarrow c \\ u \leftarrow u + d \end{cases}
 \end{aligned}
 \tag{1}$$

where V is the membrane potential, U the recovery variable, g_{AMPA} and g_{GABA} the synaptic conductances, E_{AMPA} and E_{GABA} the corresponding reversal potentials, C the membrane capacity, I the baseline input current and μ the noise of the synaptic input current. Further, n_2 , n_1 , n_0 , a , b , c and d are parameters that depend on the neuron type of the corresponding population. The fixed parameters for each population are shown in Table 1. When the membrane potential V reaches 30 mV (40 mV for striatal neurons), the action potential is considered being triggered, the membrane potential V is reset to the value c and the recovery variable U is increased by d .

The noise μ of the synaptic input current fluctuates between different random fixed points introduced by changing the value SN of each neuron after every second of simulation. The values of SN are drawn from a normal distribution with a mean value (M_{SN}) of 0. The standard deviation SD_{SN} of this distribution depends on the corresponding population (Table 1). The cortex is considered having higher levels of noise in order to drive the network, and therefore, instead of a mean M_{SN} of 0 the mean value M_{SN} is drawn from a uniform distribution ranging from -5 to 5.

The striatum is modeled by two populations of 200 inhibitory spiny projection neurons. One of these populations represents the direct spiny neurons (dSN) which initiate the direct pathway through their projections to the GPI while the other population represents the indirect spiny neurons (iSN) which initiate the indirect pathway through their projections to the GPe (Figure 1). The parameters for these two neuron types were taken from the model of Humphries, Wood, and Gurney (2009). Humphries, Wood, et al. (2009) tuned and extended a medium spiny neuron model of Izhikevich (2007; for details see Humphries, Lepora, Wood, & Gurney, 2009) to replicate data of a complex multi-compartment model (Moyer, Wolf, & Finkel, 2007) which matches in vitro whole-cell recordings from medium spiny neurons within the nucleus accumbens of rats (Wolf et al., 2005).

The GPI, GPe, STN and the thalamus are modeled each by an additional population of 200 spiking neurons. For the GPI, GPe and STN populations, the parameters were taken from Thibeault and Srinivasa (2013), who got their parameters by recreating the basal ganglia model for action selection

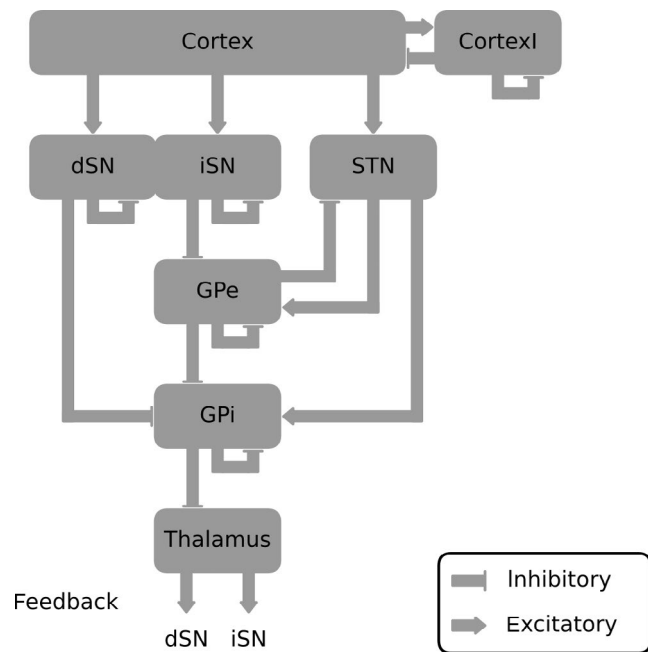


FIGURE 1 Structure of the basal ganglia model. Rectangles represent individual neuron populations. Arrows represent connections. The model consists of single spiking neuron populations for each main nuclei of the basal ganglia as described in the main text and further populations for the cortex and cortical interneurons (cortexI). With its connections, the model forms the direct (cortex–dSN–GPI), indirect (cortex–iSN–GPe–GPI and cortex–iSN–GPe–STN–GPI) and hyperdirect (cortex–STN–GPI) pathway. For each connection, the synaptic contacts of cells between the presynaptic and postsynaptic population were defined stochastically, given a connection probability. A connection probability of 1 means that every neuron of the post-population is connected with all the neurons of the pre-population. Each connection has its own weight value, which is set as the weight for all the synaptic contacts of the corresponding connection. The connection probability and weights of all connections are fitted as described in the main text. dSN—direct striatal spiny projection neurons, iSN—indirect striatal spiny projection neurons, STN—subthalamic nucleus, GPe—external globus pallidus, GPI—internal globus pallidus

of Humphries, Stewart, and Gurney (2006) with Izhikevich spiking neuron models. The model of Humphries et al. (2006) matches *in vivo* single-cell recordings and tonic firing rates from the STN and the globus pallidus of rats. Both parameter sets were also used in Baladron et al. (2019). For the thalamic population, the parameters of the phasic bursting model proposed by Izhikevich (2004) were used. The values of all cell parameters are given in Table 1.

Following our previous modeling approach Baladron et al. (2019), the GPe projects to the GPI and has reciprocal connections with the STN. The GPI combines excitatory input from the STN with the inhibitory input from both the dSN and the GPe and provides a constant inhibition to the thalamus. Further, the thalamus provides feedback to all striatal cells, thus closing a basal ganglia–thalamus loop (Hunnicutt

et al., 2016; Parent & Parent, 2004; Sadikot, Parent, & Francois, 1992; Sidibé, Bevan, Bolam, & Smith, 1997; Smith et al., 2014). Additionally, local inhibitory connections were included in the GPI, GPe, dSN and iSN population.

The cortex is modeled by two populations: one excitatory and one inhibitory. The excitatory population is composed of 600 neurons while the inhibitory of 150, following the observed proportion between cortical projection cells and interneurons. For both populations, the parameters of the tonic spiking model proposed by Izhikevich (2004) were used. The populations form an excitatory–inhibitory loop, with connection probabilities and weights set by the optimization process. The excitatory cortical cells project to all striatal cells and to the STN.

Synaptic contacts of cells between nuclei were defined stochastically, given a connection probability determined by the optimization procedure. We use conductance-based synapses in our neuron models. Therefore, the synaptic current of a cell depends on the reversal potential (E_{SYN}) and the synaptic conductance (g_{SYN}) of the individual synapses. Excitatory connections are modeled by AMPA synapses and inhibitory connections by GABA synapses. A positive AMPA conductance drives the membrane potential to the value of $E_{\text{AMPA}} = 0$ mV and the GABA conductance drives the membrane potential to the value of $E_{\text{GABA}} = -90$ mV. The conductances of these synapses decay exponentially, with time constants $\tau_{\text{AMPA}} = 10$ ms and $\tau_{\text{GABA}} = 10$ ms (see Equation 1). The rise of the synaptic conductance after a pre-synaptic action potential is modeled as an instantaneous increase by the weight value of the connection.

The neuro-computational model has been implemented using the ANNarchy neural simulator (Vitay, Dinkelbach, & Hamker, 2015; version 4.6.9b). To solve the differential equations of the model, the Euler method is used with a time step of 0.1 ms.

2.3 | BOLD signal computation

The BOLD signal is computed using the Balloon model as described by Friston, Mechelli, Turner, and Price (2000); however, as shown in Table 2, some parameters, including the time constant of the BOLD signal, have been selected from Friston, Harrison, and Penny (2003). Previous studies motivated that the neural input (synaptic activity) is a better predictor of the BOLD signal than the output signal (Logothetis, Pauls, Augath, Trinath, & Oeltermann, 2001; Mathiesen, Caesar, Akgören, & Lauritzen, 1998; Mathiesen, Caesar, & Lauritzen, 2000). Therefore, and similar to recent studies (Schmidt et al., 2018), our BOLD signal computation relies on the synaptic activity (Figure 2). The procedure used has been included into ANNarchy. A new type of monitor was added which can be attached to neuron populations in order to obtain a simulated BOLD signal. First, synaptic activity is computed at the single neuron level:

$$\tau_{\text{syn}} \frac{ds_j}{dt} = -s_j$$

if presynaptic action potential occurs, then $s_j \leftarrow s_j + \frac{1}{n_{\text{aff},j}}$

(2)

Each neuron has its own synaptic activity s_j . It decays exponentially, with the time constant $\tau_{\text{syn}} = 1$ ms. Whenever a presynaptic action potential reaches a neuron (no matter if excitatory or inhibitory), its synaptic activity s_j is increased by 1 divided by the number of all afferent synaptic contacts $n_{\text{aff},j}$ of this neuron. The theoretical maximum increase in s_j in one

TABLE 2 Parameterization of the balloon model implemented in ANNarchy

Parameter	Value	Source
E_0	0.3424	Corresponds to ρ in Friston et al. (2003)
V_0	0.02	Friston et al. (2000), Friston et al. (2003)
τ_0	1.0368	Corresponds to τ in Friston et al. (2003)
A	0.3215	Friston et al. (2003)
κ	0.665	Friston et al. (2003), corresponds to $1/\tau_s$ in Friston et al. (2000)
γ	0.412	Friston et al. (2003), corresponds to $1/\tau_f$ in Friston et al. (2000)
ϵ	1.0	

Note: The parameters were selected based on table 1 in Friston et al. (2003). The τ_0 is the time constant of the BOLD signal.

time step is therefore 1 (if presynaptic action potentials would occur at all synaptic contacts simultaneously). The calculation of the synaptic activity of a given region S_R is described by Equation 3.

$$S_R = \sum_{p \in R} \frac{1}{N_p} \sum_j^{N_p} s_j + \varphi_R \quad (3)$$

It is calculated as the sum of all mean synaptic activities of the neuron populations belonging to the region $p \in R$ with population sizes N_p . Only the striatum region (dSN and iSN) and the cortex region (excitatory and inhibitory) consist of more than one neuron population. Finally, before feeding the synaptic activity S_R into the Balloon model to produce the BOLD signal of the region, a noise value φ_R (randomly drawn every second from a uniform distribution between 0 and 0.05) is added to the synaptic activity S_R in order to model the noise affecting the BOLD signal.

2.4 | Fitting procedure

For each subject, a functional connectivity for the left and for the right hemisphere of the brain was available. We fitted our model to the functional connectivity of each hemisphere of a subject independently resulting in 15 controls for the left side and 15 more for the right side and 20 patients for the left side and 20 more for the right side.

To fit the model to the functional connectivity of a subject (patient/control, left/right), we used the Bayesian Adaptive Direct Search (BADs) algorithm (Acerbi & Ji, 2017). This

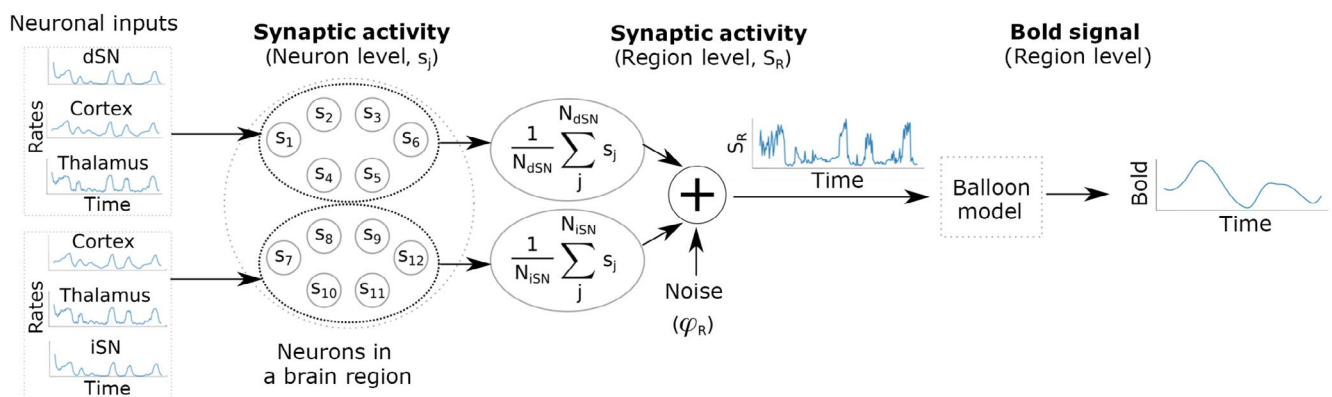


FIGURE 2 Simplified scheme of how the BOLD signal in a particular region is computed from the neural activity targeting this region. We take here the example of the striatum region. First, the rate activity in the cortex, dSN, iSN and thalamus targeting the cells in the striatum (top dSN, bottom iSN) is shown. For simplicity, we only plot 6 neurons of the dSN and iSN (12 small circles). How the synaptic activity s_j changes at the single neuron level is described in the main text. For each population of the region (here dSN and iSN), the mean of the synaptic activities s_j is calculated. Then, the means of the populations are added to obtain the synaptic activity S_R of the region (here the striatum). Finally, the obtained synaptic activity in the striatum, with the addition of noise (φ_R), is sent to the Balloon model which computes the BOLD signal for the striatum (see the plot with the BOLD signal over time). The plots are obtained from simulating the model for 20 s and recording spikes, synaptic activity and bold signal 10 times per second. dSN—direct striatal spiny projection neurons, iSN indirect striatal spiny projection neurons

TABLE 3 Overview of the different simulation paradigms

	Fitting simulation	Resting-state simulation
Cortical drive	$I = 50$ $M_{SN} = \text{uniform}(-5, 5)$	$I = 7$ $M_{SN} = 0$
Simulation procedure	Initial simulation = 15 s Simulations duration = 250 s	Initial simulation = 5 s Simulation duration = 10 s
Analyzed data	Pearson correlation matrices of the BOLD time series of all BOLD regions	Spike trains of all populations

is a general model-fitting tool and a free MATLAB package. For the fitting of each functional connectivity, we carried out 20 optimization processes with BADS. Each optimization process consisted of multiple optimization steps.

In an optimization step, BADS first selected the values of the 19 weights and probabilities. Then, a 250 s fitting simulation with the model was carried out, in which for each second, BOLD signal values of the cortex, STN, striatum, GPi, GPe and thalamus were stored, resulting in six BOLD time series. Then, the Pearson correlation matrix between these six signals was computed, which is the functional connectivity of the model. Finally, the loss value was obtained as defined in Equations 4 and 5:

$$D = FC_M - FC_S \quad (4)$$

$$\text{loss} = \left(\sum_{ij} |D_{ij}|^2 \right)^{1/2} \quad (5)$$

where the loss is the Frobenius norm of the difference (D) between the functional connectivity of the model (FC_M) and the functional connectivity of the subject (FC_S).

In each optimization process, BADS runs multiple optimization steps, each with different values for the 38 connectivity parameters, until the loss value converges to a minimum. In each of the 20 optimization processes, different initial values were randomly drawn for the 38 parameters. The probabilities and weights were initialized from a random uniform distribution ranging from 0.1 to 0.3 and from 0.005 to 0.01, respectively. The parameter values were limited in the range between 0.1 and 0.5 for the probabilities and between 0.005 and 0.015 for the weights. Finally, for each subject, we selected the 38 connectivity parameters of the optimization process that resulted in the lowest loss value.

2.5 | Rest period simulations

We compared the obtained individual models between the different groups (PD patients and controls) with respect to

the mean firing rates at rest. Therefore, additional simulations were performed with the models (see Table 3 for an overview).

To obtain the mean firing rates at rest, a 15-s resting period was simulated for each model (fitted to a specific subject). The same seed value was set for all simulations. Thus, the simulations differed only in the fitted connection parameters. The cortex input current in these simulations was set to $I = 7$. In addition, the random mean cortical firing rate fluctuations have been deactivated by setting the mean value of the normal distribution from which the noise values SN are drawn to a constant value of 0, as with the other populations. Thus, ensuring that the cortex population has an average firing rate around 10–15 Hz, which is common for neurons of the motor cortex at rest (Velliste et al., 2014).

2.6 | Sensitivity analysis

There are many predefined neuron parameters (Table 1) in our model. Although most of them are well motivated by previous studies (Humphries, Lepora, et al., 2009; Thibault & Srinivasa, 2013), it is unlikely that these parameters are exactly like those of the individual human subjects. Variations in the predefined parameters may affect the values of the fitted connectivity parameters. Therefore, we conducted a sensitivity analysis in which we varied all the predefined non-zero parameters of Table 1 to estimate how sensitive our results are to variations. Although the parameters of the neuron types of the excitatory (cortex) and inhibitory (cortexI) cortical neurons are given separately in Table 1, we used the same parameter values for cortexI as for cortex, except for I and SD , which are always zero for cortexI. As it was not possible for us to investigate how the predefined parameters would affect the fitted connectivity parameters due to the long duration of the fitting procedure (over one month for the 70 fitted models), we only investigated the sensitivity of the loss of the already fitted models. For each fitted model, we varied each of the 59 parameters from -5% to $+5\%$ in 0.3125% increments of its value specified in Table 1 while leaving the other 58 parameters constant. The simulation procedure was the same as in the

fitting simulations (Fitting simulation, Table 3) and differed only in parameter initialization. The connectivity parameters (weights and probabilities) were not randomly initialized instead the parameter values obtained by the previous optimization procedure for each fitted model were used. Further in each simulation, one predefined parameter deviated from its standard value as described above.

3 | RESULTS

3.1 | Fitting results

Models fitted to the left and right hemispheres of each subject are treated as individual models for the control and patient group in the analyses, providing us with 30 control and 40 patient models. Examples of experimental and their corresponding fitted functional connectivities of two control and two patient subjects are shown in Figure 3. The mean loss of all the fitted functional connectivities is $M = 1.10$ with a standard deviation of $SD = 0.20$. Further, we calculated the pairwise correlation (Pearson correlation coefficient) between each fitted and the corresponding experimental functional connectivity. The mean correlation of all the fitted functional connectivities is $M = 0.89$ with a standard deviation of $SD = 0.04$.

To verify if the fitted models can be clustered into different groups of models (control/patient), we tested if the control models fit significantly better to the experimental control data than to the experimental patient data and vice versa for the patient models. Thus, for each group (controls/patients) we calculated the losses between the functional connectivities of the models and the mean experimental functional connectivity (MEFC) of both groups, according to Equation 4. Then for each group of models, we compared the losses obtained from the control MEFC with the losses obtained from the patient MEFC by performing an one-tailed t test for dependent

samples. The significance of the two tests was determined with a significance level of $\alpha = 0.05$ and further Bonferroni correction. As shown in Table 4, the functional connectivities of the control models have a significantly lower loss to the control MEFC than to the patient MEFC and vice versa for the patient models, meaning that our fitting processes led to two different groups of models.

3.2 | Comparison between patient and control models

In order to compare our results with the popular rate model of PD (Albin et al., 1989; DeLong, 1990), we computed the connection strengths between nuclei as a multiplication of weight value and connection probability. We compared the connection strengths of the control group with the connection strengths of the patient group by a two-tailed t test for independent samples. The significance of the resulting 19 tests was determined using the false discovery rate (FDR) method (Benjamini & Hochberg, 1995) with a significance level of $\alpha = 0.05$. The results are shown in Table 5. Several significant differences in the connection strengths were found. Almost all significant differences have large effects according to the Cohen's d greater than 0.8 everywhere. Most connections were stronger in the patient group. Looking at the connection strengths in the direct, indirect and hyperdirect pathway, all three pathways were stronger in the Parkinsonian models. In the direct pathway, the dSN–GPi connection strength was increased by 69.4% and in the hyperdirect pathway the cortex–STN connection strength was increased by 22.9%. Especially noticeable were the differences in the indirect pathway. The increase in the cortex–iSN connection strength was particularly high at 110.2% and had also by far the largest effect size at 1.75. Further, the GPe–STN connection strength was increased by 81.5% and the GPe–GPi connection strength by 33.0%.

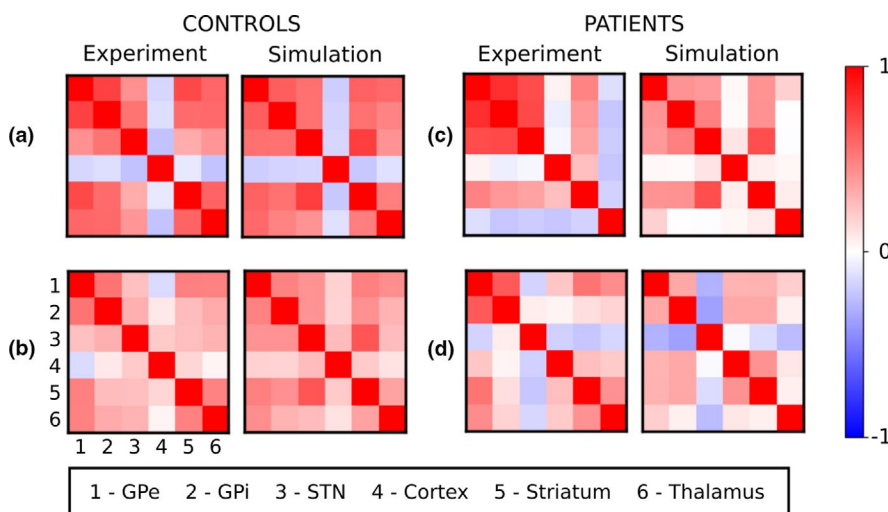


FIGURE 3 Examples for experimental and simulated functional connectivities (BOLD correlation matrices) of the corresponding fitted models. (a) and (b) show the correlation matrices of two control subjects, left experimental, right simulated. (c) and (d) show the correlation matrices of two PD patients, left experimental, right simulated. The different examples illustrate that the model was able to reproduce different shapes of correlation matrices

TABLE 4 The fitting results

	$M_c (SD_c)$	$M_p (SD_p)$	t	df	p	d
Control models	1.02 (0.25)	1.52 (0.24)	-6.54	29	<.001*	2.03
Patient models	1.89 (0.48)	1.26 (0.22)	7.81	39	<.001*	-1.66

Note: M_c/SD_c are the means/standard deviations of the losses between the functional connectivities of the models and the mean experimental functional connectivity of the control group. M_p/SD_p are the means/standard deviations of the losses between the functional connectivities of the models and the mean experimental functional connectivity of the patient group. An one-tailed t -test for dependent samples was made to compare these two samples. A * indicates significance after Bonferroni correction for a significance level of $\alpha = 0.05$.

TABLE 5 The mean connection strengths

Connection	$M_c (SD_c)$ e-3	$M_p (SD_p)$ e-3	t	df	p	d
dSN-GPi	1.93 (1.30)	3.27 (1.81)	-3.38	68	.001*	0.85
iSN-GPe	3.56 (0.98)	3.80 (1.70)	-0.70	68	.486	0.18
GPe-STN	1.46 (0.53)	2.65 (1.23)	-4.91	68	<.001*	1.26
STN-GPe	4.51 (0.78)	3.66 (1.18)	3.38	68	.001*	-0.85
STN-GPi	3.52 (0.64)	3.06 (1.30)	1.78	68	.079	-0.46
GPe-GPi	2.30 (0.65)	3.06 (1.16)	-3.20	68	.002*	0.81
GPe-GPe	2.34 (0.70)	3.25 (0.84)	-4.70	68	<.001*	1.17
GPi-GPi	3.78 (0.65)	4.02 (1.79)	-0.69	68	.492	0.18
GPi-Thalamus	1.98 (0.84)	3.32 (1.20)	-5.18	68	<.001*	1.30
Thalamus-iSN	1.30 (1.10)	2.98 (1.64)	-4.78	68	<.001*	1.20
Thalamus-dSN	1.82 (1.25)	3.45 (2.04)	-3.83	68	<.001*	0.97
dSN-dSN	3.56 (0.66)	3.64 (1.63)	-0.25	68	.805	0.06
iSN-iSN	3.02 (0.51)	2.50 (0.78)	3.16	68	.002*	-0.80
Cortex-dSN	1.78 (0.39)	2.12 (1.03)	-1.71	68	.092	0.44
Cortex-iSN	1.36 (0.74)	2.86 (0.95)	-7.03	68	<.001*	1.75
Cortex-STN	2.27 (0.43)	2.79 (1.05)	-2.53	68	.014*	0.65
Cortex-CortexI	4.13 (0.52)	3.96 (1.40)	0.62	68	.540	-0.16
CortexI-Cortex	2.74 (0.68)	3.69 (0.98)	-4.52	68	<.001*	1.14
CortexI-CortexI	3.27 (0.65)	3.87 (1.26)	-2.37	68	.020*	0.61

Note: M_c/SD_c are the means/standard deviations of the connection strengths of all models of the control group. M_p/SD_p are the means/standard deviations of the connection strengths of all models of the patient group. A two-tailed t -test for independent samples was made to compare these two samples. A * indicates significance after FDR correction for a significance level of $\alpha = 0.05$.

To obtain mean firing rates at rest, a 15-s rest period was simulated with each model. The last 10 s of these 15-s rest periods were used to obtain the mean firing rates. To calculate the mean firing rate of a region, the number of spikes, which occurred in the respective population, was divided by the time and population size. We compared the mean firing rates between the control and patient models by a two-tailed t test for independent samples for each region. The significance of the resulting 8 tests was determined using the FDR method (Benjamini & Hochberg, 1995) with a significance level of $\alpha = 0.05$. The results are shown in Table 6. The relative changes of the mean firing rates and connection strengths from the control group to the patient group are summarized in Figure 4. For the mean firing rates, several significant

differences with medium or large effect sizes were found. Mostly, the mean firing rates were lower in the patient group models. Particularly, high reductions in the mean firing rate occurred for GPe (-16.0%, Cohen's $d = -1.04$) and thalamus (-31.9%, Cohen's $d = -1.05$). Again, the iSN was especially noticeable. Here we observed by far the largest increase in the mean firing rate with a relative change of 109.8% and an effect size of 1.81.

We further investigated how homogeneous the models of the control group and the patient group were. Therefore, we calculated the coefficient of variation (CV) of the mean firing rates and of the connectivity strengths for each group. The CV value results from dividing the standard deviation by the mean of a sample. The CV values of the control and

Population	$M_c (SD_c)$	$M_p (SD_p)$	t	df	p	d
Cortex	13.21 (0.46)	12.80 (0.90)	2.24	68	.029*	-0.57
CortexI	33.30 (2.97)	30.36 (7.79)	1.93	68	.058	-0.50
dSN	22.10 (2.29)	25.90 (9.96)	-2.02	68	.047	0.53
iSN	15.99 (8.46)	33.55 (10.79)	-7.27	68	<.001*	1.81
GPe	34.84 (4.56)	29.28 (6.07)	4.15	68	<.001*	-1.04
GPI	36.28 (1.21)	34.71 (2.86)	2.77	68	.007*	-0.71
STN	27.95 (2.36)	29.02 (6.73)	-0.83	68	.412	0.21
Thalamus	18.50 (4.05)	12.60 (6.87)	4.13	68	<.001*	-1.05

Note: M_c/SD_c are the means/standard deviations of the mean firing rates at rest of all models of the control group. M_p/SD_p are the means/standard deviations of the mean firing rates at rest of all models of the patient group. A two-tailed t -test for independent samples was made to compare these two samples. A * indicates significance after FDR correction for a significance level of $\alpha = 0.05$.

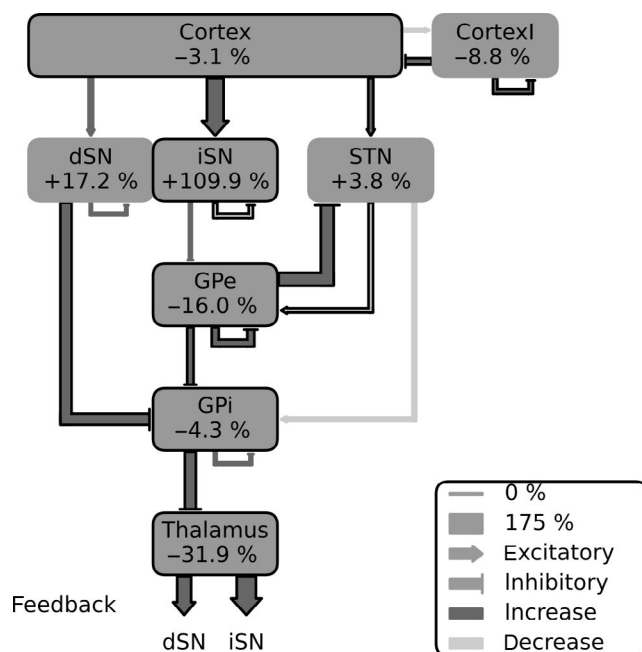


FIGURE 4 The relative changes of the mean firing rates and connectivity strengths. The numbers below each region name represent the relative change of the mean firing rate from the control group to the patient group. The relative change in connectivity strength is represented for each connection by the line thickness and color. The line color shows the direction of the changes. Dark gray indicate positive changes (increase of connectivity strength), light gray negative changes (decrease of connectivity strength). The line thickness shows the amount of the relative change, the thicker the more the connectivity strength changed. A black border around connections or regions indicates a significant difference in the mean firing rate at rest or mean connectivity strength between the control and patient group

patient group for all the regions and connections are shown in Tables 7, 8, 9, and 10. To compare the CV values between the control and patient groups, a two-tailed t test for dependent samples was performed. The changes of all the individual

TABLE 6 The mean resting firing rates

TABLE 7 The coefficients of variation of the mean firing rates or connectivity strengths of the components of the direct pathway for the control group (CV_C) and the Parkinsonian group (CV_P)

Region/connection	CV_C	CV_P	ΔCV
SD1	0.10	0.38	0.28
dSN-dSN	0.19	0.45	0.26
Cortex-dSN	0.22	0.48	0.26
dSN-GPi	0.67	0.55	-0.12
M	0.30	0.47	0.17

Note: ΔCV shows the change from the control to the Parkinsonian group.

TABLE 8 The coefficients of variation of the mean firing rates or connectivity strengths of the components of the indirect pathway for the control group (CV_C) and the Parkinsonian group (CV_P)

Region/connection	CV_C	CV_P	ΔCV
GPe	0.13	0.21	0.08
STN	0.08	0.23	0.15
iSN	0.53	0.32	-0.21
GPe-GPe	0.30	0.26	-0.04
iSN-iSN	0.17	0.31	0.15
Cortex-iSN	0.55	0.33	-0.21
GPe-GPi	0.28	0.38	0.10
STN-GPi	0.18	0.42	0.24
iSN-GPe	0.28	0.45	0.17
GPe-STN	0.37	0.46	0.10
M	0.29	0.34	0.05

Note: ΔCV shows the change from the control to the Parkinsonian group.

CV values of the connectivity strengths and mean firing rates are illustrated in Figure 5. The mean of all CV values was significantly larger in the patient group than in the control group ($t_{57} = -2.66$, $p = .013$, Cohen's $d = 0.49$). Thus, the

models of the patient group were more heterogeneous. To investigate the heterogeneity of the different pathways, we calculated the mean CV values for each pathway from all its components (shown in Tables 7, 8 and 9). All pathways were more heterogeneous in the patient group. The indirect pathway had a mean ΔCV of 0.05 and thus the smallest increase of heterogeneity. The direct pathway with a mean CV value of 0.47 was the most heterogeneous pathway in the patient group models. The cortex–iSN connection and the iSN rate were more homogeneous instead of more heterogeneous in the patient group; thus, the increased activity of iSN cells was very common in the Parkinsonian models.

3.3 | Sensitivity analysis

In the sensitivity analysis, we obtained the loss values calculated from the differences between the functional connectivities of controls/PD patients and the functional connectivities of the corresponding fitted models (see Equations 4 and 5) for different parameter variations in the fitted models. For each parameter, which was varied, we calculated the relative change in the loss depending on the change of the parameter value. This was done for each of the 70 models. 90% of all loss changes over all models and parameter deviations were smaller than $\pm 16\%$. They ranged from -43% to $+363\%$. For each parameter, we calculated the standard deviation of the corresponding loss values. The loss values of the two parameters with the highest standard deviation ($SD_{\text{cortex n1}} = 0.64$, $SD_{\text{thalamus n1}} = 0.59$) and the two parameters with the lowest standard deviations ($SD_{\text{STN I}} = 0.05$, $SD_{\text{thalamus a}} = 0.05$) are shown in Figure 6. For cortex n1 and thalamus n1, the loss increased on average with increasing parameter deviation, but in some models, there was almost no change or even a reduction of the loss. Positive and negative parameter deviations did not have exactly the same effect but if the loss changed on average, it increased for both positive and negative parameter deviations. Thus, to indicate how sensitive the loss is to each individual parameter, we fitted a linear regression model without an intercept to predict the relative loss changes of all models using the absolute values of the relative parameter deviations. The slope coefficient obtained

TABLE 9 The coefficients of variation of the mean firing rates or connectivity strengths of the components of the hyperdirect pathway for the control group (CV_C) and the Parkinsonian group (CV_P)

Region/connection	CV_C	CV_P	ΔCV
STN	0.08	0.23	0.15
Cortex-STN	0.19	0.38	0.19
STN-GPi	0.18	0.42	0.24
<i>M</i>	0.15	0.34	0.19

Note: ΔCV shows the change from the control to the Parkinsonian group.

for each parameter indicated by what percentage the average loss of the models changed due to a 1% parameter deviation.

TABLE 10 The coefficients of variation of the mean firing rates or connectivity strengths of the components which do not belong to one of the three pathways for the control group (CV_C) and the Parkinsonian group (CV_P)

Region/connection	CV_C	CV_P	ΔCV
Cortex	0.03	0.07	0.04
CortexI	0.09	0.26	0.17
Thalamus	0.22	0.55	0.33
CortexI-Cortex	0.25	0.27	0.02
STN-GPe	0.17	0.32	0.15
CortexI-CortexI	0.20	0.33	0.13
Cortex-CortexI	0.13	0.35	0.23
GPe-Thalamus	0.42	0.36	-0.06
GPe-GPi	0.17	0.45	0.27
Thalamus-iSN	0.85	0.55	-0.30
Thalamus-dSN	0.69	0.59	-0.10
<i>M</i>	0.29	0.37	0.08

Note: ΔCV shows the change from the control to the Parkinsonian group.

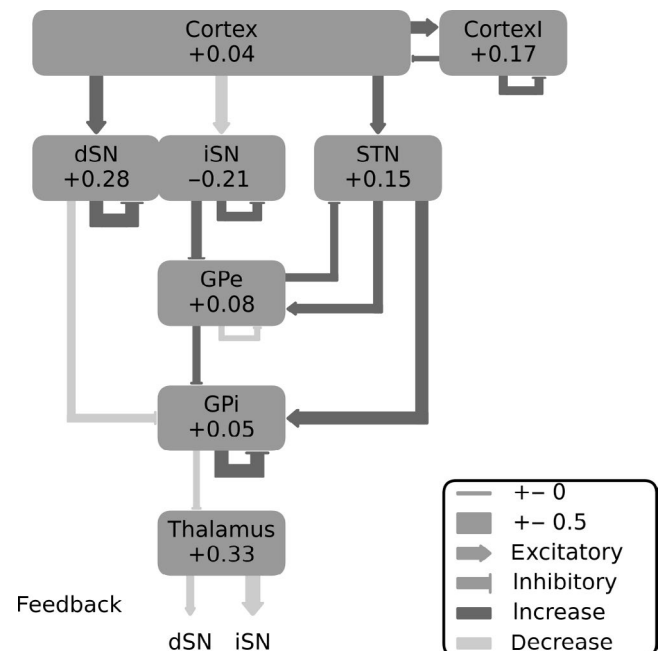


FIGURE 5 Differences in CV values. The figure shows the absolute changes in CV values for each connectivity strength and the mean firing rate of the populations. The numbers below each region name represent the absolute change of the CV value of the mean firing rate from the control group to the patient group. The absolute change in the CV values of the connectivity strengths is represented for each connection by the line thickness and color. The line color shows the direction of the changes. Dark gray are increases, light gray are decreases. The line thickness shows the amount of the relative change, the thicker the more the CV value changed

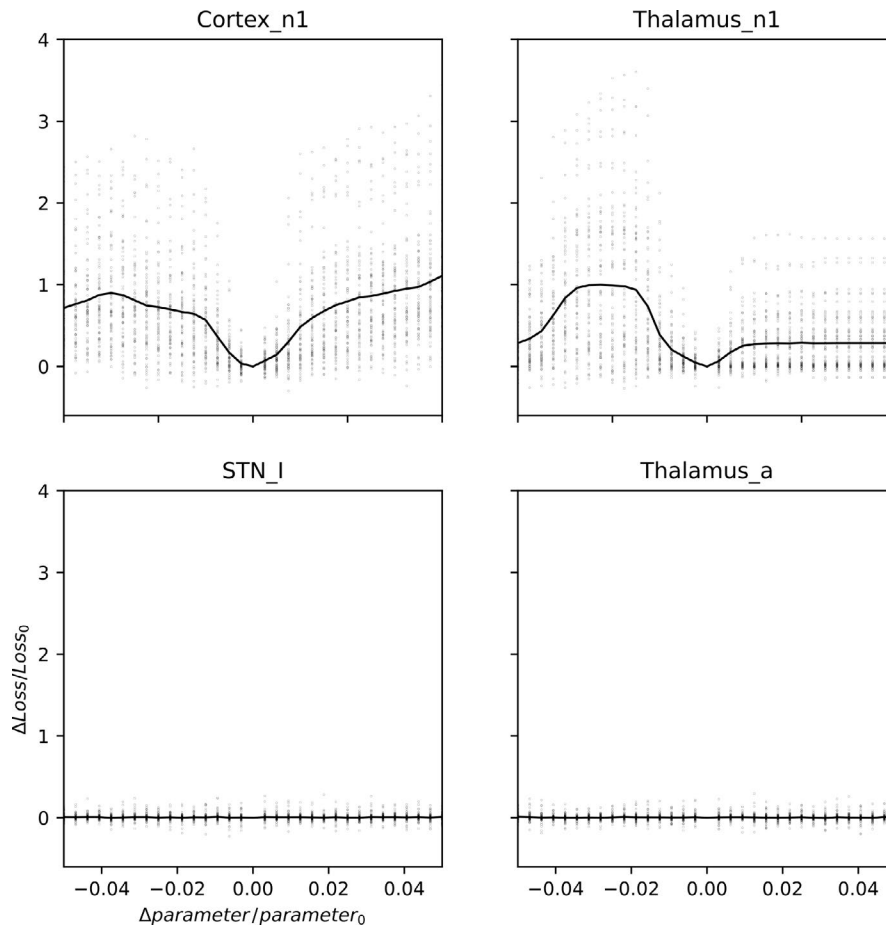


FIGURE 6 Relative loss changes depending on relative deviations of four example parameters, cortex n1, cortex n2, striatum n1 and striatum n2. Each observation is presented by a small circle. The data were collected over the 70 fitted models; thus, there are 70 observations for each parameter variation. The 33 parameter variations ranging from -5% to $+5\%$ in 0.3125% increments. The black line indicates the mean over the 70 models. The plots are quite symmetrical and thus show that the change of the loss depends mainly on the absolute value of the relative parameter deviation. $\Delta Loss$ —absolute loss change of the corresponding model, $Loss_0$ —loss value of the corresponding model with standard parameters from Table 1

The slope coefficients for all the parameters are shown in Figure 7. They ranged from 0.12 to 23.61 with a median of 0.19. The median indicated that most slope coefficients were quite low. Regarding the different neuron populations, parameter deviations in the cortex and thalamus population in particular had a strong influence on the loss. This is probably because the cortex drives the entire model and the thalamus has a very similar influence through its feedback connections to the striatum. In terms of the various parameters, n_0 , n_1 and n_2 , which were specified by (Izhikevich, 2003), clearly had the strongest effect. These are the parameters of the quadratic membrane potential equation, which therefore have a direct influence on the activity of the neurons.

4 | DISCUSSION

We have used a primarily data-driven approach to generate changes related to PD in a subject-specific basal ganglia computational model, based on the assumption that Parkinsonian and control models differ in their functional connectivity strengths. By tuning the connection strength and synapse density of each connection in our model to match the functional connectivity obtained from the model with the functional connectivity of individual control subjects and

PD patients, we obtained individual basal ganglia models of healthy controls and PD patients. This allowed us to compare these two groups of models in terms of individual connection strengths and mean firing rates at rest.

Many computational studies already investigated PD with basal ganglia models (reviews, Humphries et al., 2018; Schroll & Hamker, 2016). However, these models were not fit to data of healthy and PD subjects (Holgado, Terry, & Bogacz, 2010; Kumar, Cardanobile, Rotter, & Aertsen, 2011; Lindahl & Kotaleski, 2016; Mandali, Rengaswamy, Chakravarthy, & Moustafa, 2015; McCarthy et al., 2011; Terman, Rubin, Yew, & Wilson, 2002). To compare healthy and PD states in basal ganglia models, the most common approach so far is to implement the modulatory effects of DA into the model, where DA is either an external variable (Guthrie, Myers, & Gluck, 2009; Humphries et al., 2006; Leblois, Boraud, Meissner, Bergman, & Hansel, 2006; Lindahl & Kotaleski, 2016) or implemented within the model by neurons representing the SNc activity (Frank, 2005; Schroll, Vitay, & Hamker, 2014). States of DA then differentially affect the activity of striatal spiny projection neurons or the degree of long-term potentiation or depression. Thus, the predictions made by these neuro-computational models with respect to how PD changes processing in the basal ganglia critically depend on assumptions about the effects of DA in the basal ganglia built into the models.

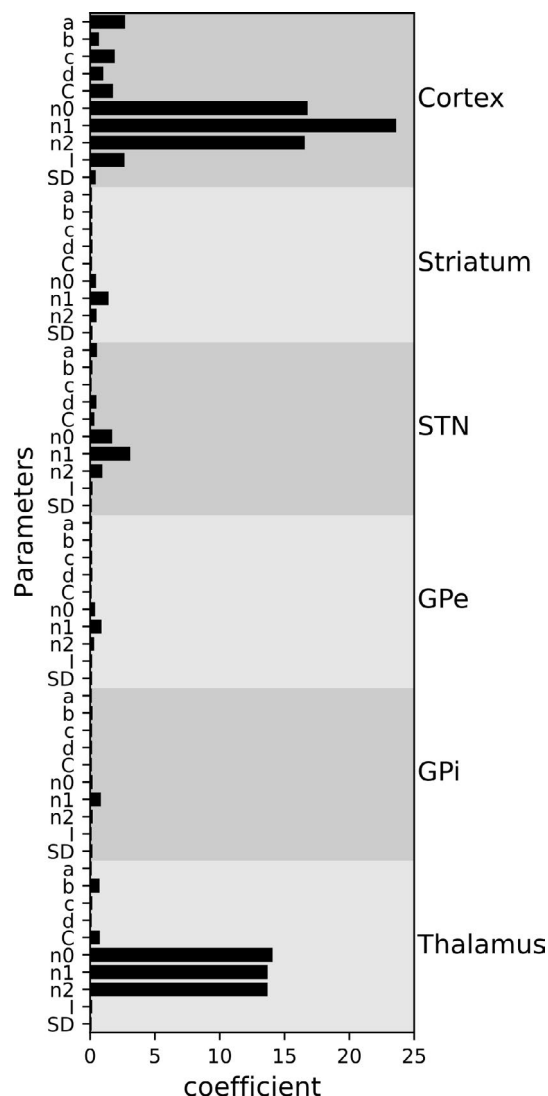


FIGURE 7 Slope coefficients of the linear regression model predicting the relative loss changes using the absolute values of the relative parameter deviations. The data were collected over the 70 fitted models and 33 parameter variations ranging from -5% to $+5\%$ in 0.3125% increments for each parameter. The slope coefficient of each parameter is shown by the width of the vertical bars. The background colors indicate the corresponding population of the parameters

4.1 | The “rate model” of PD and corresponding neurophysiological findings

Due to the popularity of the so-called rate model of the basal ganglia, particularly the version of DeLong (1990), we compared the individual predictions of this rate model and our results with respect to experimental findings compiled in several reviews (DeLong & Wichmann, 2009; Galvan et al., 2015; Galvan & Wichmann, 2008; Lee & Masmanidis, 2019; McGregor & Nelson, 2019; Obeso & Lanciego, 2011; Obeso et al., 2000; Wichmann & Delong, 2002).

The rate model suggests that DA activates the dSN cells of the direct pathway and inhibits the iSN cells of the indirect

pathway. Due to the reduction of DA in PD, iSN cells become more active which leads to a stronger inhibition of GPe, whereupon the STN is disinhibited. The hyperactive STN then causes a stronger stimulation of the GPi. In addition, the DA loss reduces the activity of the dSN cells, whereby the GPi is additionally disinhibited. Convergingly, this leads to a hyperactive GPi, resulting in a strong inhibition of the thalamus, whereby the cortex receives less excitatory input from the thalamus. The inhibited thalamus and the less excited or less responsive cortex are proposed to result in bradykinesia.

Although we have not implemented modulation by DA or DA changes in our models, similarities between the results of our study and the predictions of the rate model are apparent. The most consistent change that occurred in the Parkinsonian models was the stronger cortex–iSN connection and higher iSN firing rate. Despite some variability in experimental observations, more active iSN cells seem to be a very consistent finding in experimental studies. Increased firing rates were measured in PD animal models (Kita & Kita, 2011; Mallet, Ballion, Le Moine, & Gonon, 2006; Sharott, Vinciati, Nakamura, & Magill, 2017), and further findings on synapse density (Day et al., 2006), increased metabolism in GPe (Crossman, Mitchell, & Sambrook, 1985; Mitchell, Cross, Sambrook, & Crossman, 1986; Schwartzman & Alexander, 1985) and increased GABA levels in GPe (Bianchi, Galeffi, Bolam, & Della Corte, 2003; Robertson, Graham, Sambrook, & Crossman, 1991) indicate increased activity of the iSN cells. Only a few studies did not reproduce an increased iSN firing rate in PD (Ketzer et al., 2017; Ryan, Bair-Marshall, & Nelson, 2018).

Further, our model predicts a lower firing rate in GPe. Also, these changes were reported in many animal model studies (Boraud, Bezard, Guehl, Bioulac, & Gross, 1998; Fillion & Tremblay, 1991; Miller & DeLong, 1987, 1988; Pan & Walters, 1988; Schwartzman & Alexander, 1985; Soares et al., 2004) but a few reports argue against it, like Bezard, Boraud, Bioulac, and Gross (1999), which observed an increase in STN but no decrease in GPe firing rate.

Our Parkinsonian models showed lower firing rates in the thalamus, as supported by many previous findings (Kammermeier, Pittard, Hamada, & Wichmann, 2016; Molnar, Pilliar, Lozano, & Dostrovsky, 2005; Ni, Gao, Benabid, & Benazzouz, 2000; Schneider & Rothblat, 1996; Vitek, Ashe, & Kaneoke, 1994). However, the findings for the thalamus are quite inconsistent (Galvan et al., 2015) including findings of no rate change (Pessiglione et al., 2005) or even increased rates (Bosch-Bouju, Smither, Hyland, & Parr-Brownlie, 2014). Concurrently, the thalamus in our PD models had the most heterogeneous mean firing rates. In fact, some PD patients’ models showed mean thalamus firing rates above 20 Hz, which is higher than in some controls’ models. Therefore, our results also suggest that some PD patients may have an increased rather than a decreased thalamus firing rate.

A further consistency of our results with the predictions of the rate model is the decreased firing rates of the cortex, which were previously demonstrated in studies on monkeys (Pasquereau, DeLong, & Turner, 2016; Pasquereau & Turner, 2011). According to the rate model, the reduced activity of the cortex should result from the excessively inhibited thalamus. This cannot be the case in our model as we closed the loop via the thalamus. As we have drastically simplified the cortex in our model and have neglected cortical inputs like cortex–thalamus loops, it is unlikely that our model plausibly explains why the cortex has a lower activity. Furthermore, the difference in the cortical firing rate is relatively small in our models.

In some points, our findings contradict estimations of the rate model. First, the activity of the dSN in our PD models is higher than the rate model would predict. We do not observe a significant decrease in the PD group models but even the opposite tendency. However, there are some sparse findings in the literature that describe increased dSN firing rates in PD (Kita & Kita, 2011; Mallet et al., 2006; Ryan et al., 2018) albeit they are less frequent than findings of dSN decreased rates. Some studies show that the metabolism in the GPi is increased (Crossman et al., 1985; Schwartzman & Alexander, 1985). This is usually understood to be resulting from increased input from the hyperactive STN. However, the increased metabolism could also be a consequence of increased afferent synaptic activity caused by the dSN cells. In addition, our results show that cortex–dSN connectivity strength, dSN firing rate and dSN–GPi connectivity strength are among the most heterogeneous effects in our Parkinsonian models.

Second, contradicting predictions of the rate model our findings indicate a less active GPi in PD. Although strongly debated, GPi overactivity predicted by the rate model has been partially supported by some studies (Boraud et al., 1998; Fillion & Tremblay, 1991; Miller & DeLong, 1987, 1988; Soares et al., 2004; Wichmann et al., 1999). Findings on increased metabolism in the thalamus also suggest an increased inhibitory input from the GPi (Mitchell et al., 1989; Rolland et al., 2007). However, these findings could also speak for a stronger GPi–thalamus connection, as was the case in our Parkinsonian models. Nevertheless, the findings of previous studies do not indicate that the GPi is less active in PD.

Finally, the STN should be overactive according to the rate model. STN overactivity was found in several studies (Benazzouz et al., 2002; Bergman, Wichmann, Karmon, & DeLong, 1994; Bezard et al., 1999; Hassani, Mouroux, & Feger, 1996; Kreiss, Mastropietro, Rawji, & Walters, 1997; Miller & DeLong, 1987; Soares et al., 2004; Vila et al., 2000). In our Parkinsonian models, the STN only showed a tendency toward hyperactivity, but no significant effect. Increased metabolism in GPe and GPi also indicate an overactive STN (Crossman et al., 1985; Mitchell et al., 1986; Schwartzman

& Alexander, 1985), but also unaltered STN firing rates in Parkinsonian rodents have been reported (Delaville, McCoy, Gerber, Cruz, & Walters, 2015).

In summary, our data-driven approach illustrates PD changes similar to predictions of the rate model, which are in coherence with many experimental findings. This suggests a certain plausibility of the rate changes in our models, which result exclusively from fitting functional connectivity of patients and healthy controls. However, there are also some inconsistencies in our data with the rate model predictions, especially the lower firing rates in GPi and the lack of increased firing rates in STN.

The data to which our models were fitted were collected during active dopaminergic medication of the PD patients (Horn et al., 2019). This medication may have affected basal ganglia firing rates, which should be considered when interpreting our results. Levy et al. (2001) showed that DA agonist apomorphine administration leads to a generally lower GPi rate and a lower STN rate during movement in PD patients. This could be a reason why we did not find an increased STN or GPi rate in our models. In addition, the DBS electrodes implanted in the patients despite being switched off probably caused artifacts in the BOLD signal, especially in the STN signal, which reduces the validity of our results about the STN.

4.2 | Firing rates to explain PD

So far, we have only compared findings, which suggest or show certain neuronal activity changes with our results and the rate model. Of course, the rate model does not only describe the rates themselves, but also tries to explain PD symptoms by changes in the rates. Meanwhile, it has been shown that the predictions the rate model makes about the effects of certain rate changes on motor function cannot be replicated very consistently (DeLong & Wichmann, 2009; Galvan & Wichmann, 2008; Obeso & Lanciego, 2011; Wichmann & DeLong, 2002) and other features such as firing pattern with prolonged bursts and pauses are most likely more important as a simple output rate (Hutchison et al., 1994; Levy, Hutchison, Lozano, & Dostrovsky, 2000; Molnar et al., 2005; Vitek et al., 1999; Wichmann & Soares, 2006). Moreover, invasive recordings in humans via DBS electrodes over the last two decades have shown that abnormal oscillatory activity in the cortico-BG network is related to motor symptoms such as increased beta band activity in PD bradykinesia and rigidity (Kühn & Volkmann, 2017).

We, therefore, do not want to draw any direct conclusions about the symptoms in PD with our findings on the rate changes. Rather, our study should be seen as a proof of concept, in that we obtained plausible rate changes, in

accordance with many experimental findings, solely from the functional connectivity data of controls and patients.

4.3 | Limitations

Our approach is complementary to previous neuro-computational accounts to study the effects of PD in the basal ganglia. Most importantly, it directly relies on data from both, control subjects and PD patients, it requires no specific assumptions of how DA deficiency associated with PD changes processing in the model and it leads to subject-specific neuro-computational models at the level of spiking activity. However, we shall also mention the limitations of the present design. Although we are able to bridge scales from BOLD data to neural spiking dynamics, one has to be aware that the free model parameters are tuned to match BOLD correlation data. Thus, no direct access to firing rates or local field potentials exists that could further constrain the model. Given BOLD data, the model is already fairly complex, but certainly far away from the true biological detail, as several neuron types and their connectivity are not included. An important prerequisite for the validity of our results is that the differences in functional connectivity between patients and controls were caused by PD. This is not completely fulfilled in our data. Even though the subjects were age-matched, the data were collected in two different laboratories. The patients' data were scanned at 3 T, and the controls' data were scanned at 1.5 T. In addition, the patients received a DBS electrode which may cause artifacts in the BOLD signal even when switched off. Besides the free parameters obtained by the optimization process, our model has a large number of fixed parameters that were not optimized by the optimization process. Our sensitivity analysis shows that some of these parameters have a strong influence on the losses of the models. Thus, changes in these parameters could also cause changes in our results. However, it is important to remember that these parameters should not be arbitrarily different from ours. Most of our parameters were chosen based on previous studies (Humphries, Lepora, et al., 2009; Izhikevich, 2004; Thibeault & Srinivasa, 2013) to mimic the firing properties of the respective neurons based on physiological data. The optimal case would be to have access to the specific parameters for each individual patient and control subject, but this would require single-cell recordings for all the different nuclei for each patient and control subject, which would not be feasible. Thus, we took a compromise and combined general assumptions (e.g., the neuron models/firing properties) with easily accessible individual data (like MRI) to obtain individual models. Despite these limitations, we found a good match to existing data as outlined above, although present data are also quite variable.

However, not each prediction of the model should be interpreted literally. While the increase in iSN activity is very consistent among the subject-specific models of PD and also observed in recent studies (Kita & Kita, 2011; Mallet et al., 2006; Sharott et al., 2017), the massive increase in iSN firing rate is likely an overestimation. Thus, despite the promising observations, future studies should explore how to add additional constraints to the model or add more data to the optimization procedure. Our approach used in this study could be further extended with more complex models, albeit there is a limitation in the number of parameters being fit. Models that would replicate the neuronal mechanisms relevant for PD symptoms can then also be used to investigate treatment options for PD in more detail. As the method used in this study provides models of both, healthy and Parkinsonian states, it offers a promising environment to systematically search for treatments that bring the Parkinsonian models closer to the healthy ones. In addition, the method provides individual models of patients, a potential that has not been exploited in our present study. With individual models, tailored PD treatments could be investigated, comparable to the "virtual epileptic patient" (Jirsa et al., 2017). This might help to plan and improve treatment efficacy for the heterogeneous PD phenotypes.

5 | CONCLUSION

The approach to fit functional connectivity data with a spiking neuro-computational basal ganglia model and thus inferring firing rates and connectivity strengths has proven to be quite successful. We have indeed found many similarities with the rate model of the basal ganglia and corresponding recent physiological findings. Our results show quite meaningful changes in firing rates in the basal ganglia, associated with PD. These changes emerged only due to differences in the functional connectivity of PD patients and controls and were thus obtained without implementing effects of DA and DA changes associated with PD in the models. As firing rates alone have become somewhat outdated in terms of explaining PD symptoms, in the future, our approach could be further developed to include effects of synchrony, oscillations and bursts in PD, by using additional data in the fitting procedure. In addition, our study is a confident first step toward obtaining subject-specific models from non-invasive imaging data of PD patients and healthy controls that could be useful for tailored treatments of PD.

ACKNOWLEDGEMENTS

This work was supported by the German Research Foundation DFG HA2630/11-1 part of "Computational Connectomics" (SPP 2041). This work was supported by the SMARTSTART Programme of the Bernstein Network

and Volkswagen Foundation. Data used in the preparation of this article were obtained from the Parkinson's Progression Markers Initiative (PPMI) database (www.ppmi-info.org/data). For up-to-date information on the study, visit www.ppmi-info.org. PPMI—a public-private partnership—is funded by the Michael J. Fox Foundation for Parkinson's Research and funding partners, see www.ppmi-info.org/fundingpartners.

CONFLICT OF INTEREST

The authors declare no competing interests.

AUTHOR CONTRIBUTIONS

Designed research: FH, JB; Performed research: OM, FV; Guided research: FH, JB; Programming: JB, FV, HD, OM; Data analysis: OM; Acquired funding: FH, AH, AK; Writing (1st draft): OM, FV, JB; Writing (reviewing and editing): FH, JB, AH, FI, AK; Providing experimental data: AH, FI, AK.

DATA AVAILABILITY STATEMENT

Our study is theoretical (computational modeling). We did not collect any data.

ORCID

Oliver Maith  <https://orcid.org/0000-0002-6446-9110>

Francesc Villagrasa Escudero  <https://orcid.org/0000-0003-0149-6231>

Helge Ülo Dinkelbach  <https://orcid.org/0000-0002-8871-8177>

Andreas Horn  <https://orcid.org/0000-0002-0695-6025>

Friederike Irmen  <https://orcid.org/0000-0001-5574-3790>

Andrea A. Kühn  <https://orcid.org/0000-0002-4134-9060>

Fred H. Hamker  <https://orcid.org/0000-0001-9104-7143>

REFERENCES

- Acerbi, L., & Ji, W. (2017). Practical Bayesian optimization for model fitting with Bayesian adaptive direct search. In I. Guyon, U. Luxburg, S. Bengio, H. Wallach, R. Fergus, S. Vishwanathan, & R. Garnett (Eds.), *Advances in neural information processing systems*, 30. Presented at the 2017 Conference on Neural Information Processing Systems (pp. 1836–1846). New York, NY: Curran Associates, Inc.
- Albin, R. L., Young, A. B., & Penney, J. B. (1989). The functional anatomy of basal ganglia disorders. *Trends in Neurosciences*, 12, 366–375.
- Baladron, J., Nambu, A., & Hamker, F. H. (2019). The subthalamic nucleus-external globus pallidus loop biases exploratory decisions towards known alternatives: A neuro-computational study. *European Journal of Neuroscience*, 49, 754–767. <https://doi.org/10.1111/ejn.13666>
- Benazzouz, A., Breit, S., Koudsie, A., Pollak, P., Krack, P., & Benabid, A.-L. (2002). Intraoperative microrecordings of the subthalamic nucleus in Parkinson's disease. *Movement Disorders*, 17, S145–S149. <https://doi.org/10.1002/mds.10156>
- Benjamini, Y., & Hochberg, Y. (1995). Controlling the false discovery rate: A practical and powerful approach to multiple testing. *Journal of the Royal Statistical Society: Series B Methodology*, 57, 289–300.
- Bergman, H., Wichmann, T., Karmon, B., & DeLong, M. (1994). The primate subthalamic nucleus. II. Neuronal activity in the MPTP model of Parkinsonism. *Journal of Neurophysiology*, 72, 507–520.
- Bernheimer, H., Birkmayer, W., Hornykiewicz, O., Jellinger, K., & Seitelberger, F. (1973). Brain dopamine and the syndromes of Parkinson and Huntington Clinical, morphological and neurochemical correlations. *Journal of the Neurological Sciences*, 20, 415–455.
- Bezard, E., Boraud, T., Bioulac, B., & Gross, C. E. (1999). Involvement of the subthalamic nucleus in glutamatergic compensatory mechanisms. *European Journal of Neuroscience*, 11, 2167–2170.
- Bianchi, L., Galeffi, F., Bolam, J., & Della Corte, L. (2003). The effect of 6-hydroxydopamine lesions on the release of amino acids in the direct and indirect pathways of the basal ganglia: A dual microdialysis probe analysis. *European Journal of Neuroscience*, 18, 856–868. <https://doi.org/10.1046/j.1460-9568.2003.02795.x>
- Biswal, B., Zerrin Yetkin, F., Haughton, V. M., & Hyde, J. S. (1995). Functional connectivity in the motor cortex of resting human brain using echo-planar MRI. *Magnetic Resonance in Medicine*, 34, 537–541.
- Boraud, T., Bezard, E., Guehl, D., Bioulac, B., & Gross, C. (1998). Effects of L-DOPA on neuronal activity of the globus pallidus externalis (GPe) and globus pallidus internalis (GPi) in the MPTP-treated monkey. *Brain Research*, 787, 157–160. [https://doi.org/10.1016/S0006-8993\(97\)01563-1](https://doi.org/10.1016/S0006-8993(97)01563-1)
- Bosch-Bouju, C., Smither, R. A., Hyland, B. I., & Parr-Brownlie, L. C. (2014). Reduced reach-related modulation of motor thalamus neural activity in a rat model of Parkinson's disease. *Journal of Neuroscience*, 34, 15836–15850.
- Brookes, M. J., Woolrich, M., Luckhoo, H., Price, D., Hale, J. R., Stephenson, M. C., ... Morris, P. G. (2011). Investigating the electrophysiological basis of resting state networks using magnetoencephalography. *Proceedings of the National Academy of Sciences*, 108, 16783–16788.
- Cabral, J., Fernandes, H. M., Van Hartevelt, T. J., James, A. C., Kringelbach, M. L., & Deco, G. (2013). Structural connectivity in schizophrenia and its impact on the dynamics of spontaneous functional networks. *Chaos: an Interdisciplinary Journal of Nonlinear Science*, 23, 046111.
- Crossman, A., Mitchell, I., & Sambrook, M. (1985). Regional brain uptake of 2-deoxyglucose in N-methyl-4-phenyl-1, 2, 3, 6-tetrahydropyridine (MPTP)—induced Parkinsonism in the macaque monkey. *Neuropharmacology*, 24, 587–591. [https://doi.org/10.1016/0028-3908\(85\)90070-X](https://doi.org/10.1016/0028-3908(85)90070-X)
- Day, M., Wang, Z., Ding, J., An, X., Ingham, C. A., Shering, A. F., ... Surmeier, D. J. (2006). Selective elimination of glutamatergic synapses on striatopallidal neurons in Parkinson disease models. *Nature Neuroscience*, 9, 251–259. <https://doi.org/10.1038/nn1632>
- Deco, G., & Jirsa, V. K. (2012). Ongoing cortical activity at rest: Criticality, multistability, and ghost attractors. *Journal of Neuroscience*, 32, 3366–3375. <https://doi.org/10.1523/JNEUROSCI.2523-11.2012>
- Deco, G., Ponce-Alvarez, A., Mantini, D., Romani, G. L., Hagmann, P., & Corbetta, M. (2013). Resting-state functional connectivity emerges from structurally and dynamically shaped slow linear fluctuations. *Journal of Neuroscience*, 33, 11239–11252.
- Delaville, C., McCoy, A. J., Gerber, C. M., Cruz, A. V., & Walters, J. R. (2015). Subthalamic nucleus activity in the awake hemiparkinsonian rat: Relationships with motor and cognitive networks. *Journal of Neuroscience*, 35, 6918–6930. <https://doi.org/10.1523/JNEUROSCI.0587-15.2015>

- DeLong, M. R. (1990). Primate models of movement disorders of basal ganglia origin. *Trends in Neurosciences*, 13, 281–285.
- DeLong, M., & Wichmann, T. (2009). Update on models of basal ganglia function and dysfunction. *Parkinsonism & Related Disorders*, 15, S237–S240. [https://doi.org/10.1016/S1353-8020\(09\)70822-3](https://doi.org/10.1016/S1353-8020(09)70822-3)
- Filion, M., & Tremblay, L. (1991). Abnormal spontaneous activity of globus pallidus neurons in monkeys with MPTP-induced Parkinsonism. *Brain Research*, 547, 140–144.
- Frank, M. J. (2005). Dynamic dopamine modulation in the basal ganglia: A neurocomputational account of cognitive deficits in medicated and nonmedicated Parkinsonism. *Journal of Cognitive Neuroscience*, 17, 51–72. <https://doi.org/10.1162/0898929052880093>
- Friston, K. J. (2011). Functional and effective connectivity: A review. *Brain Connectivity*, 1, 13–36.
- Friston, K. J., Harrison, L., & Penny, W. (2003). Dynamic causal modelling. *NeuroImage*, 19, 1273–1302. [https://doi.org/10.1016/S1053-8119\(03\)00202-7](https://doi.org/10.1016/S1053-8119(03)00202-7)
- Friston, K. J., Mechelli, A., Turner, R., & Price, C. J. (2000). Nonlinear responses in fMRI: The Balloon model, Volterra kernels, and other hemodynamics. *NeuroImage*, 12, 466–477. <https://doi.org/10.1006/nimg.2000.0630>
- Galvan, A., Devergnas, A., & Wichmann, T. (2015). Alterations in neuronal activity in basal ganglia-thalamocortical circuits in the parkinsonian state. *Frontiers in Neuroanatomy*, 9, 5.
- Galvan, A., & Wichmann, T. (2008). Pathophysiology of Parkinsonism. *Clinical Neurophysiology*, 119, 1459–1474.
- Guthrie, M., Myers, C., & Gluck, M. (2009). A neurocomputational model of tonic and phasic dopamine in action selection: A comparison with cognitive deficits in Parkinson's disease. *Behavioral Brain Research*, 200, 48–59. <https://doi.org/10.1016/j.bbr.2008.12.036>
- Hassani, O.-K., Mouroux, M., & Feger, J. (1996). Increased subthalamic neuronal activity after nigral dopaminergic lesion independent of disinhibition via the globus pallidus. *Neuroscience*, 72, 105–115. [https://doi.org/10.1016/0306-4522\(95\)00535-8](https://doi.org/10.1016/0306-4522(95)00535-8)
- He, B. J., Snyder, A. Z., Zempel, J. M., Smyth, M. D., & Raichle, M. E. (2008). Electrophysiological correlates of the brain's intrinsic large-scale functional architecture. *Proceedings of the National Academy of Sciences*, 105, 16039–16044.
- He, Y., Wang, J., Wang, L., Chen, Z. J., Yan, C., Yang, H., ... Evans, A. C. (2009). Uncovering intrinsic modular organization of spontaneous brain activity in humans. *PLoS One*, 4, e5226. <https://doi.org/10.1371/journal.pone.0005226>
- Holgado, A. J. N., Terry, J. R., & Bogacz, R. (2010). Conditions for the generation of beta oscillations in the subthalamic nucleus–globus pallidus network. *Journal of Neuroscience*, 30, 12340–12352.
- Horn, A., Wenzel, G., Irmen, F., Huebl, J., Li, N., Neumann, W.-J., ... Kühn, A. A. (2019). Deep brain stimulation induced normalization of the human functional connectome in Parkinson's disease. *Brain*, 142, 3129–3143. <https://doi.org/10.1093/brain/awz239>
- Humphries, M. D., Lepora, N., Wood, R., & Gurney, K. (2009). Capturing dopaminergic modulation and bimodal membrane behaviour of striatal medium spiny neurons in accurate, reduced models. *Frontiers in Computational Neuroscience*, 3, 26. <https://doi.org/10.3389/neuro.10.026.2009>
- Humphries, M. D., Obeso, J. A., & Dreyer, J. K. (2018). Insights into Parkinson's disease from computational models of the basal ganglia. *Journal of Neurology, Neurosurgery and Psychiatry*, 89, 1181–1188.
- Humphries, M. D., Stewart, R. D., & Gurney, K. N. (2006). A physiologically plausible model of action selection and oscillatory activity in the basal ganglia. *Journal of Neuroscience*, 26, 12921–12942.
- Humphries, M. D., Wood, R., & Gurney, K. (2009). Dopamine-modulated dynamic cell assemblies generated by the GABAergic striatal microcircuit. *Neural Networks*, 22, 1174–1188. <https://doi.org/10.1016/j.neunet.2009.07.018>
- Hunnicutt, B. J., Jongbloets, B. C., Birdsong, W. T., Gertz, K. J., Zhong, H., & Mao, T. (2016). A comprehensive excitatory input map of the striatum reveals novel functional organization. *Elife*, 5, e19103. <https://doi.org/10.7554/eLife.19103>
- Hutchison, W., Lozano, A., Davis, K., Saint-Cyr, J., Lang, A., & Dostrovsky, J. (1994). Differential neuronal activity in segments of globus pallidus in Parkinson's disease patients. *NeuroReport*, 5, 1533–1537.
- Izhikevich, E. M. (2003). Simple model of spiking neurons. *IEEE Transactions on Neural Networks*, 14, 1569–1572.
- Izhikevich, E. M. (2004). Which model to use for cortical spiking neurons? *IEEE Transactions on Neural Networks*, 15, 1063–1070.
- Izhikevich, E. M. (2007). *Dynamical systems in neuroscience*. Cambridge, MA: MIT Press.
- Jankovic, J. (2008). Parkinson's disease: Clinical features and diagnosis. *Journal of Neurology, Neurosurgery and Psychiatry*, 79, 368–376.
- Jirsa, V. K., Proix, T., Perdikis, D., Woodman, M. M., Wang, H., Gonzalez-Martinez, J., ... Bartolomei, F. (2017). The virtual epileptic patient: Individualized whole-brain models of epilepsy spread. *NeuroImage*, 145, 377–388. <https://doi.org/10.1016/j.neuroimage.2016.04.049>
- Kammermeier, S., Pittard, D., Hamada, I., & Wichmann, T. (2016). Effects of high-frequency stimulation of the internal pallidal segment on neuronal activity in the thalamus in parkinsonian monkeys. *Journal of Neurophysiology*, 116, 2869–2881. <https://doi.org/10.1152/jn.00104.2016>
- Ketzel, M., Spigolon, G., Johansson, Y., Bonito-Oliva, A., Fisone, G., & Silberberg, G. (2017). Dopamine depletion impairs bilateral sensory processing in the striatum in a pathway-dependent manner. *Neuron*, 94, 855–865. <https://doi.org/10.1016/j.neuron.2017.05.004>
- Kita, H., & Kita, T. (2011). Role of striatum in the pause and burst generation in the globus pallidus of 6-OHDA-treated rats. *Frontiers in Systems Neuroscience*, 5, 42.
- Kreiss, D. S., Mastropietro, C. W., Rawji, S. S., & Walters, J. R. (1997). The response of subthalamic nucleus neurons to dopamine receptor stimulation in a rodent model of Parkinson's disease. *Journal of Neuroscience*, 17, 6807–6819.
- Kühn, A. A., & Volkmann, J. (2017). Innovations in deep brain stimulation methodology. *Movement Disorders*, 32, 11–19.
- Kumar, A., Cardanobile, S., Rotter, S., & Aertsen, A. (2011). The role of inhibition in generating and controlling Parkinson's disease oscillations in the basal ganglia. *Frontiers in Systems Neuroscience*, 5, 86.
- Leblois, A., Boraud, T., Meissner, W., Bergman, H., & Hansel, D. (2006). Competition between feedback loops underlies normal and pathological dynamics in the basal ganglia. *Journal of Neuroscience*, 26, 3567–3583.
- Lee, K., & Masmanidis, S. C. (2019). Aberrant features of in vivo striatal dynamics in Parkinson's disease. *Journal of Neuroscience Research*, 97, 1678–1688.
- Levy, R., Dostrovsky, J., Lang, A., Sime, E., Hutchison, W., & Lozano, A. (2001). Effects of apomorphine on subthalamic nucleus and globus pallidus internus neurons in patients with Parkinson's disease. *Journal of Neurophysiology*, 86, 249–260.

- Levy, R., Hutchison, W. D., Lozano, A. M., & Dostrovsky, J. O. (2000). High-frequency synchronization of neuronal activity in the subthalamic nucleus of parkinsonian patients with limb tremor. *Journal of Neuroscience*, 20, 7766–7775.
- Lindahl, M., & Kotaleski, J. H. (2016). Untangling basal ganglia network dynamics and function: Role of dopamine depletion and inhibition investigated in a spiking network model. *Eneuro*, 3, ENEURO.0156–16.2016. <https://doi.org/10.1523/ENEURO.0156-16.2016>
- Logothetis, N. K., Pauls, J., Augath, M., Trinath, T., & Oeltermann, A. (2001). Neurophysiological investigation of the basis of the fMRI signal. *Nature*, 412, 150–157. <https://doi.org/10.1038/35084005>
- Maia, T. V., & Frank, M. J. (2011). From reinforcement learning models to psychiatric and neurological disorders. *Nature Neuroscience*, 14, 154.
- Mallet, N., Ballion, B., Le Moine, C., & Gonon, F. (2006). Cortical inputs and GABA interneurons imbalance projection neurons in the striatum of parkinsonian rats. *Journal of Neuroscience*, 26, 3875–3884.
- Mandali, A., Rengaswamy, M., Chakravarthy, V. S., & Moustafa, A. A. (2015). A spiking Basal Ganglia model of synchrony, exploration and decision making. *Frontiers in Neuroscience*, 9, 191.
- Marek, K., Jennings, D., Lasch, S., Siderowf, A., Tanner, C., Simuni, T., ... Taylor, P. (2011). The Parkinson progression marker initiative (PPMI). *Progress in Neurobiology*, 95, 629–635.
- Mathiesen, C., Caesar, K., Akgören, N., & Lauritzen, M. (1998). Modification of activity-dependent increases of cerebral blood flow by excitatory synaptic activity and spikes in rat cerebellar cortex. *Journal of Physiology*, 512, 555–566. <https://doi.org/10.1111/j.1469-7793.1998.555be.x>
- Mathiesen, C., Caesar, K., & Lauritzen, M. (2000). Temporal coupling between neuronal activity and blood flow in rat cerebellar cortex as indicated by field potential analysis. *Journal of Physiology*, 523, 235–246.
- McCarthy, M., Moore-Kochlacs, C., Gu, X., Boyden, E., Han, X., & Kopell, N. (2011). Striatal origin of the pathologic beta oscillations in Parkinson's disease. *Proceedings of the National Academy of Sciences*, 108, 11620–11625.
- McGregor, M. M., & Nelson, A. B. (2019). Circuit mechanisms of Parkinson's disease. *Neuron*, 101, 1042–1056. <https://doi.org/10.1016/j.neuron.2019.03.004>
- Miller, W. C., & DeLong, M. R. (1987). Altered tonic activity of neurons in the globus pallidus and subthalamic nucleus in the primate MPTP model of Parkinsonism. In M. Carpenter, & A. Jayaraman (Eds.), *The Basal Ganglia II* (pp. 415–427). New York, NY: Plenum.
- Miller, W. C., & DeLong, M. R. (1988). Parkinsonian symptomatology. An anatomical and physiological analysis. *Annals of the New York Academy of Sciences*, 515, 287–302.
- Mitchell, I., Clarke, C., Boyce, S., Robertson, R., Peggs, D., Sambrook, M., & Crossman, A. (1989). Neural mechanisms underlying Parkinsonian symptoms based upon regional uptake of 2-deoxyglucose in monkeys exposed to 1-methyl-4-phenyl-1, 2, 3, 6-tetrahydropyridine. *Neuroscience*, 32, 213–226. [https://doi.org/10.1016/0306-4522\(89\)90120-6](https://doi.org/10.1016/0306-4522(89)90120-6)
- Mitchell, I., Cross, A., Sambrook, M., & Crossman, A. (1986). Neural mechanisms mediating 1-methyl-4-phenyl-1, 2, 3, 6-tetrahydropyridine-induced Parkinsonism in the monkey: Relative contributions of the striatopallidal and striatonigral pathways as suggested by 2-deoxyglucose uptake. *Neuroscience Letters*, 63, 61–65. [https://doi.org/10.1016/0304-3940\(86\)90013-3](https://doi.org/10.1016/0304-3940(86)90013-3)
- Molnar, G. F., Pilliar, A., Lozano, A. M., & Dostrovsky, J. O. (2005). Differences in neuronal firing rates in pallidal and cerebellar receiving areas of thalamus in patients with Parkinson's disease, essential tremor, and pain. *Journal of Neurophysiology*, 93, 3094–3101. <https://doi.org/10.1152/jn.00881.2004>
- Moyer, J. T., Wolf, J. A., & Finkel, L. H. (2007). Effects of dopaminergic modulation on the integrative properties of the ventral striatal medium spiny neuron. *Journal of Neurophysiology*, 98, 3731–3748.
- Nambu, A., Tachibana, Y., & Chiken, S. (2015). Cause of parkinsonian symptoms: Firing rate, firing pattern or dynamic activity changes? *Basal Ganglia*, 5, 1–6. <https://doi.org/10.1016/j.baga.2014.11.001>
- Ni, Z., Gao, D., Benabid, A., & Benazzouz, A. (2000). Unilateral lesion of the nigrostriatal pathway induces a transient decrease of firing rate with no change in the firing pattern of neurons of the parafascicular nucleus in the rat. *Neuroscience*, 101, 993–999. [https://doi.org/10.1016/S0306-4522\(00\)00337-7](https://doi.org/10.1016/S0306-4522(00)00337-7)
- Obeso, J. A., & Lanciego, J. L. (2011). Past, present, and future of the pathophysiological model of the Basal Ganglia. *Frontiers in Neuroanatomy*, 5, 39.
- Obeso, J. A., Rodriguez-Oroz, M. C., Rodriguez, M., Lanciego, J. L., Artieda, J., Gonzalo, N., & Olanow, C. W. (2000). Pathophysiology of the basal ganglia in Parkinson's disease. *Trends in Neurosciences*, 23, S8–S19. [https://doi.org/10.1016/S1471-1931\(00\)00028-8](https://doi.org/10.1016/S1471-1931(00)00028-8)
- Pan, H. S., & Walters, J. R. (1988). Unilateral lesion of the nigrostriatal pathway decreases the firing rate and alters the firing pattern of globus pallidus neurons in the rat. *Synapse (New York, N. Y.)*, 2, 650–656. <https://doi.org/10.1002/syn.890020612>
- Parent, M., & Parent, A. (2004). The pallidofugal motor fiber system in primates. *Parkinsonism & Related Disorders*, 10, 203–211.
- Pasquereau, B., DeLong, M. R., & Turner, R. S. (2016). Primary motor cortex of the parkinsonian monkey: Altered encoding of active movement. *Brain*, 139, 127–143. <https://doi.org/10.1093/brain/awv312>
- Pasquereau, B., & Turner, R. S. (2011). Primary motor cortex of the parkinsonian monkey: Differential effects on the spontaneous activity of pyramidal tract-type neurons. *Cerebral Cortex*, 21, 1362–1378. <https://doi.org/10.1093/cercor/bhq217>
- Pessiglione, M., Guehl, D., Rolland, A.-S., François, C., Hirsch, E. C., Féger, J., & Tremblay, L. (2005). Thalamic neuronal activity in dopamine-depleted primates: Evidence for a loss of functional segregation within basal ganglia circuits. *Journal of Neuroscience*, 25, 1523–1531. <https://doi.org/10.1523/JNEUROSCI.4056-04.2005>
- Popovich, O. V., Manos, T., Hoffstaedter, F., & Eickhoff, S. B. (2019). What can computational models contribute to neuroimaging data analytics? *Frontiers in Systems Neuroscience*, 12, 68.
- Robertson, R., Graham, W., Sambrook, M., & Crossman, A. (1991). Further investigations into the pathophysiology of MPTP-induced Parkinsonism in the primate: An intracerebral microdialysis study of γ -aminobutyric acid in the lateral segment of the globus pallidus. *Brain Research*, 563, 278–280. [https://doi.org/10.1016/0006-8993\(91\)91545-C](https://doi.org/10.1016/0006-8993(91)91545-C)
- Rolland, A.-S., Herrero, M.-T., Garcia-Martinez, V., Ruberg, M., Hirsch, E. C., & François, C. (2007). Metabolic activity of cerebellar and basal ganglia-thalamic neurons is reduced in Parkinsonism. *Brain*, 130, 265–275. <https://doi.org/10.1093/brain/awl337>

- Rubin, J. E. (2017). Computational models of basal ganglia dysfunction: The dynamics is in the details. *Current Opinion in Neurobiology*, 46, 127–135.
- Ryan, M. B., Bair-Marshall, C., & Nelson, A. B. (2018). Aberrant striatal activity in Parkinsonism and levodopa-induced dyskinesia. *Cell Reports*, 23, 3438–3446.
- Sadikot, A., Parent, A., & Francois, C. (1992). Efferent connections of the centromedian and parafascicular thalamic nuclei in the squirrel monkey: A PHA-L study of subcortical projections. *The Journal of Comparative Neurology*, 315, 137–159.
- Schirner, M., McIntosh, A. R., Jirsa, V., Deco, G., & Ritter, P. (2018). Inferring multi-scale neural mechanisms with brain network modeling. *Elife*, 7, e28927. <https://doi.org/10.7554/eLife.28927>
- Schmidt, M., Bakker, R., Shen, K., Bezgin, G., Diesmann, M., & van Albada, S. J. (2018). A multi-scale layer-resolved spiking network model of resting-state dynamics in macaque visual cortical areas. *PLoS Computational Biology*, 14, e1006359. <https://doi.org/10.1371/journal.pcbi.1006359>
- Schneider, J., & Rothblat, D. S. (1996). Alterations in intralaminar and motor thalamic physiology following nigrostriatal dopamine depletion. *Brain Research*, 742, 25–33.
- Schroll, H., & Hamker, F. H. (2016). Basal Ganglia dysfunctions in movement disorders: What can be learned from computational simulations. *Movement Disorders*, 31, 1591–1601.
- Schroll, H., Vitay, J., & Hamker, F. H. (2014). Dysfunctional and compensatory synaptic plasticity in Parkinson's disease. *European Journal of Neuroscience*, 39, 688–702.
- Schwartzman, R. J., & Alexander, G. M. (1985). Changes in the local cerebral metabolic rate for glucose in the 1-methyl-4-phenyl-1, 2, 3, 6-tetrahydropyridine (MPTP) primate model of Parkinson's disease. *Brain Research*, 358, 137–143. [https://doi.org/10.1016/0006-8993\(85\)90957-6](https://doi.org/10.1016/0006-8993(85)90957-6)
- Sharott, A., Vinciati, F., Nakamura, K. C., & Magill, P. J. (2017). A population of indirect pathway striatal projection neurons is selectively entrained to parkinsonian beta oscillations. *Journal of Neuroscience*, 37, 9977–9998.
- Sidibé, M., Bevan, M. D., Bolam, J. P., & Smith, Y. (1997). Efferent connections of the internal globus pallidus in the squirrel monkey: I. Topography and synaptic organization of the pallidothalamic projection. *The Journal of Comparative Neurology*, 382, 323–347. [https://doi.org/10.1002/\(SICI\)1096-9861\(19970609\)382:3<323::AID-CNE3>3.0.CO;2-5](https://doi.org/10.1002/(SICI)1096-9861(19970609)382:3<323::AID-CNE3>3.0.CO;2-5)
- Smith, Y., Galvan, A., Ellender, T., Doig, N., Villalba, R., Ocampo, I., ... Bolam, J. P. (2014). The thalamostriatal system in normal and diseased states. *Frontiers in Systems Neuroscience*, 8, 5.
- Soares, J., Kliem, M. A., Betarbet, R., Greenamyre, J. T., Yamamoto, B., & Wichmann, T. (2004). Role of external pallidal segment in primate Parkinsonism: Comparison of the effects of 1-methyl-4-phenyl-1, 2, 3, 6-tetrahydropyridine-induced Parkinsonism and lesions of the external pallidal segment. *Journal of Neuroscience*, 24, 6417–6426. <https://doi.org/10.1523/JNEUROSCI.0836-04.2004>
- Terman, D., Rubin, J. E., Yew, A., & Wilson, C. (2002). Activity patterns in a model for the subthalamopallidal network of the basal ganglia. *Journal of Neuroscience*, 22, 2963–2976.
- Thibeault, C. M., & Srinivasa, N. (2013). Using a hybrid neuron in physiologically inspired models of the basal ganglia. *Frontiers in Computational Neuroscience*, 7, 88.
- Van Hartevelt, T. J., Cabral, J., Deco, G., Møller, A., Green, A. L., Aziz, T. Z., & Kringelbach, M. L. (2014). Neural plasticity in human brain connectivity: The effects of long term deep brain stimulation of the subthalamic nucleus in Parkinson's disease. *PLoS One*, 9, e86496. <https://doi.org/10.1371/journal.pone.0086496>
- Velliste, M., Kennedy, S. D., Schwartz, A. B., Whitford, A. S., Sohn, J.-W., & McMorland, A. J. (2014). Motor cortical correlates of arm resting in the context of a reaching task and implications for prosthetic control. *Journal of Neuroscience*, 34, 6011–6022.
- Vila, M., Perier, C., Feger, J., Yelnik, J., Faucheux, B., Ruberg, M., ... Hirsch, E. (2000). Evolution of changes in neuronal activity in the subthalamic nucleus of rats with unilateral lesion of the substantia nigra assessed by metabolic and electrophysiological measurements. *European Journal of Neuroscience*, 12, 337–344.
- Vitay, J., Dinkelbach, H. Ü., & Hamker, F. H. (2015). ANNarchy: A code generation approach to neural simulations on parallel hardware. *Frontiers Neuroinformatics*, 9, 19.
- Vitek, J., Ashe, J., & Kaneoke, Y. (1994). Spontaneous neuronal activity in the motor thalamus: Alteration in pattern and rate in Parkinsonism. *Society for Neuroscience Abstracts*, 20, 561.
- Vitek, J. L., Chockkan, V., Zhang, J. Y., Kaneoke, Y., Evatt, M., DeLong, M. R., ... Bakay, R. A. (1999). Neuronal activity in the basal ganglia in patients with generalized dystonia and hemiballismus. *Annals of Neurology*, 46, 22–35.
- Wichmann, T., Bergman, H., Starr, P. A., Subramanian, T., Watts, R. L., & DeLong, M. R. (1999). Comparison of MPTP-induced changes in spontaneous neuronal discharge in the internal pallidal segment and in the substantia nigra pars reticulata in primates. *Experimental Brain Research*, 125, 397–409. <https://doi.org/10.1007/s002210050696>
- Wichmann, T., & DeLong, M. (2002). Neurocircuitry of Parkinson's disease. In K. Davis, D. Charney, J. Coyle, & C. Nemeroff (Eds.), *Neuropsychopharmacology: The fifth generation of progress* (pp. 1761–1779). Philadelphia, PA: Lippincott Williams & Wilkins.
- Wichmann, T., & Soares, J. (2006). Neuronal firing before and after burst discharges in the monkey basal ganglia is predictably patterned in the normal state and altered in parkinsonism. *Journal of Neurophysiology*, 95, 2120–2133. <https://doi.org/10.1152/jn.01013.2005>
- Wolf, J. A., Moyer, J. T., Lazarewicz, M. T., Contreras, D., Benoit-Marand, M., O'Donnell, P., & Finkel, L. H. (2005). NMDA/AMPA ratio impacts state transitions and entrainment to oscillations in a computational model of the nucleus accumbens medium spiny projection neuron. *The Journal of Neuroscience*, 25, 9080–9095.

How to cite this article: Maith O, Villagrasa Escudero F, Dinkelbach HÜ, et al. A computational model-based analysis of basal ganglia pathway changes in Parkinson's disease inferred from resting-state fMRI. *Eur J Neurosci*. 2021;53:2278–2295. <https://doi.org/10.1111/ejn.14868>